

pubs.acs.org/acscatalysis Research Article

Distant Oxide Surfaces Dominating Catalytic Reaction Kinetics: The Case of Pt/CeO₂

Eunwon Lee, Sungsu Kang, Arik Beck, Jungwon Park, Jaeha Lee,* and Do Heui Kim*



Cite This: ACS Catal. 2025, 15, 9477-9488



ACCESS I

III Metrics & More

Article Recommendations

s Supporting Information

ABSTRACT: One of the main goals of catalysis research is to improve the reaction efficiency by using platinum-group metals (PGMs) more effectively, given their high cost. PGMs are typically dispersed on oxide supports to maximize their surface area, under the assumption that catalytic activity arises primarily from the PGMs and their immediate oxide surroundings, while oxide surfaces located further away from PGMs are often considered catalytically irrelevant. However, a growing body of research on spillover phenomena suggests that PGMs can influence the catalytic properties of oxide surface sites located several nanome-



ters away from PGMs, prompting the question of whether distant oxide surfaces can play a more active, or even dominant, role in catalytic kinetics. A shift in understanding, from viewing the oxide surface as merely a passive support to recognizing it as an active promoter of the rate-limiting step (RLS), would offer an alternative framework for optimizing PGM utilization. In this contribution, we investigated the role of distant oxide surfaces in CO oxidation, using Pt/CeO₂ as a model system. Our findings show that distant CeO₂ surfaces are not inert but can promote the CO oxidation reaction via oxygen spillover. Interestingly, when the CeO₂ content in Pt/CeO₂ is high, the catalytic activity across catalysts with varying distributions of Pt single atoms and clusters is identical. Kinetic analysis reveals that, in CeO₂-rich Pt/CeO₂ catalysts, the RLS is the activation of oxygen on the distant CeO₂ surface. Further investigation indicated that the alignment of CeO₂ grains during reductive treatment facilitates the oxygen supply to Pt, boosting catalytic activity. This study suggests that leveraging the catalytic function of the distant oxide surface offers a promising strategy to enhance the efficiency of PGMs, providing an alternative perspective on catalyst development.

KEYWORDS: Pt, CeO₂, distant oxide surfaces, CO oxidation, O-spillover, rate-limiting step

1. INTRODUCTION

The primary objective of catalysis research is to enhance the efficiency of target reactions using cost-effective and sustainable catalysts. Platinum-group metals (PGMs) are among the most active materials for a broad range of thermocatalytic and electrocatalytic reactions; however, their high cost necessitates strategies to maximize their utilization. One common approach is to disperse PGMs onto oxide supports, thereby increasing their surface area-to-volume ratio and improving catalytic efficiency. The effectiveness of dispersed PGMs is typically evaluated by identifying active sites, usually PGMs interacting with oxides, and assessing the dispersion of these sites. Their reactivity is then measured, commonly in terms of turnover frequency (TOF), which quantifies the number of reactants converted per active site per unit time.

In PGM-oxide heterogeneous catalysts, it is commonly assumed that the active sites consist of either isolated PGM atoms or PGM ensembles, along with oxide surface sites in direct contact with, or within a few atomic distances of, the PGMs.^{1,2} Even in cases where catalytic reactivity is described by the Mars-van Krevelen mechanism, where lattice O from

the oxide support participates in the oxidation of reactants adsorbed on PGMs, the reactive O is typically modeled as originating from oxide surfaces immediately adjacent to the metal sites.^{3–5} As a result, oxide domains located several nanometers away from PGMs are often considered catalytically inactive or treated as mere spectators in the overall reaction process.

However, numerous studies on spillover phenomena, such as H- or O-spillover, have demonstrated that these processes can facilitate the catalytic reactions at oxide surface sites located several nanometers away from adjacent PGMs. The idea that spillover can modulate catalytic reactivity has a long and well-established history. Since the first report in 1964 on Pt-promoted WO₃ reduction, seminal works in the 1990s advanced the concept that the donor phase (e.g., sites capable

Received: March 1, 2025 Revised: May 5, 2025 Accepted: May 13, 2025



of supplying spillover species such as H or O by dissociating $\rm H_2$ or $\rm O_2$) can influence the activity and selectivity of a spatially separated catalytic phase. ¹⁶ Notable examples include reactions such as selective oxidation and dehydrogenation, where O-spillover plays a critical role, a phenomenon aptly termed "remote control." ^{17,18} These early studies not only demonstrated that spillover species could impact reactivity over nanometer-scale distances, but also showed that incorporating spillover into kinetic models enabled accurate prediction of catalytic behavior, successfully capturing the synergistic effects between spatially distinct active sites. Since then, an expanding body of experimental and theoretical work has provided increasingly rigorous evidence for spillover chemistry and has helped elucidate its underlying physicochemical characteristics.

In light of this extensive history, it is important to consider whether spillover phenomena contribute to the overall catalytic activity in PGM-supported oxide systems. Specifically, oxide domains located spatially distant from PGMs may still play a critical role in modulating catalytic activity through spillover processes. This question is particularly relevant given that PGMs typically occupy less than 10% of the catalyst surface, with the majority of the exposed area consisting of PGM-free oxide support. Accurately determining the contribution of these remote oxide surfaces is therefore essential for developing reliable structure—function relationships. If such surfaces are shown to significantly influence reactivity, it would prompt a fundamental reassessment of how the "active site" is defined and spatially characterized in catalyst systems.

In this study, by detailed kinetic and structural characterization, we investigated the catalytic contribution of CeO₂ surfaces located a few nm away from PGMs by examining the CO oxidation activity of Pt/CeO₂ catalysts as a model system. Pt/CeO₂ catalysts have been extensively studied to understand the synergistic interactions between PGMs and oxides. 4,5,19-25 It has been suggested that the active sites in Pt/CeO₂ for CO oxidation are composed of Pt species, ranging from single atoms (SAs) and Pt clusters to metallic Pt nanoparticles, interacting with CeO₂ surface sites in close proximity to Pt. However, the potential catalytic role of CeO₂ surfaces several nm away from Pt has been generally overlooked, despite the known effect of O-spillover on CeO2 surfaces, potentially enabling distant CeO₂ surfaces to participate in the reaction. 26-28 Interestingly, we found that Pt/CeO2 catalysts with different Pt structures, ranging from varying distributions of Pt SAs to clusters of different sizes, but identical Pt-to-CeO₂ mass ratios and an excess of CeO2 exhibited comparable catalytic activity. This suggests that the activity is not dependent on the specific distribution of Pt species under these conditions. Kinetic analysis suggests that the rate-limiting step (RLS) for CO oxidation is the dissociation of O₂ on the CeO₂ surface away from Pt. As the dilution ratio of CeO₂ to Pt/CeO₂ increases, the entropy enhancement for CO oxidation reaction, driven by the increased availability of CeO₂ sites capable of supplying O to Pt, also increased significantly. This results in catalytic activity that becomes independent of Pt structure distributions when excess distant CeO₂ surface is present. Further analysis suggests that this enhancement in activity is related to the size of CeO₂ grains with aligned lattices, composed of Pt/CeO₂ and CeO₂ grains, whose formation is promoted during reductive pretreatment. This study highlights the important role of oxide sites located away from PGMs in determining catalytic activity, an aspect that has not been fully considered and could have a profound impact on the field.

2. METHODS

- **2.1. Catalyst Preparation.** In this study, Pt weight loadings ranged from 0.5 to 4 wt % were deposited on CeO_2 (Rhodia) using the incipient wetness impregnation method. The BET surface area estimated from N_2 adsorption/desorption isotherms and crystalline size measured by X-ray powder diffraction of CeO_2 were $142 \text{ m}^2/\text{g}$ and 8.6 nm, respectively. High-purity (99.99%) $Pt(NH_3)_4(NO_3)_3$ solution (Sigma-Aldrich) was used as the Pt precursor. The impregnated catalysts were dried overnight at $100 \, ^{\circ}\text{C}$ in an oven. The dried catalysts were then calcined at $500 \, ^{\circ}\text{C}$ with $10\% \, O_2/N_2$ for 2 h in a flow reactor (ramp rate: $10 \, ^{\circ}\text{C/min}$).
- 2.2. Characterization Methods. 2.2.1. CO-Diffuse Reflectance Infrared Fourier Transform Spectroscopy (DRIFTS). In situ CO-IR spectra were collected using a Nicolet 6700 FT-IR spectrometer (Thermo Fisher Scientific) equipped with a mercury cadmium telluride (MCT) detector and a Praying Mantis diffuse reflectance cell (Harrick Scientific Products). Spectra were recorded over the range of 4000-600 cm⁻¹ with 32 scans at a resolution of 4 cm⁻¹. Approximately 0.1 g of catalyst was loaded into the DRIFTS cell and subjected to in situ pretreatment under either 10% H₂/N₂ (reductive) or 10% O_2/N_2 (oxidative) at 400 °C for 1 h. Following pretreatment, the sample was cooled to 35 °C under N₂ flow, and a background spectrum was collected. The catalyst was then exposed to 5000 ppm of CO/N2, followed by a 2 min N₂ purge to remove gas-phase and weakly adsorbed CO. The total gas flow was maintained at 100 mL/min and balanced with N_2 throughout the experiment.
- 2.2.2. X-ray Photoelectron Spectroscopy (XPS). XPS analyses were performed using a K-Alpha spectrometer (Thermo Scientific, U.K.) equipped with a monochromated Al K α X-ray source (1486.6 eV) and a 180 ° double-focusing hemispherical analyzer with a 128-channel detector. Binding energies were calibrated against the C 1s peak at 284.6 eV, attributed to adventitious carbon from atmospheric contamination
- 2.2.3. Transmission Electron Microscopy (TEM). High-angle annular dark-field (HAADF) scanning TEM (STEM) images were obtained using a JEM-ARM200F transmission electron microscope (JEOL, Japan), equipped with a spherical aberration corrector in the condenser lens (probe corrector) and a cold field emission gun. The instrument is housed at the National Center for Interuniversity Research Facilities, Seoul National University. For sample preparation, Pt/CeO₂ powders were dispersed in ethanol, and a drop of the suspension was deposited onto a lacey-C TEM grid, followed by drying in an oven at room temperature.
- 2.2.4. X-ray Powder Diffraction (XRD). XRD patterns were recorded using a SmartLab diffractometer (Rigaku, Japan) operated in Mode 1 with Cu K α radiation (λ = 1.5406 Å), at 40 kV and 30 mA. Data were collected over a 2 θ range of 10–80° with a step size of 0.02° and a scan rate of 2.5°/min.
- 2.2.5. N_2 Adsorption/Desorption Isotherms. N_2 adsorption/desorption isotherms were measured by using a BELSORP-mini II analyzer (MicrotracBEL, Japan) at liquid nitrogen temperature (-196 °C). Prior to analysis, the catalyst sample was degassed at 250 °C under vacuum for 4 h to eliminate impurities.

ACS Catalysis pubs.acs.org/acscatalysis Research Article

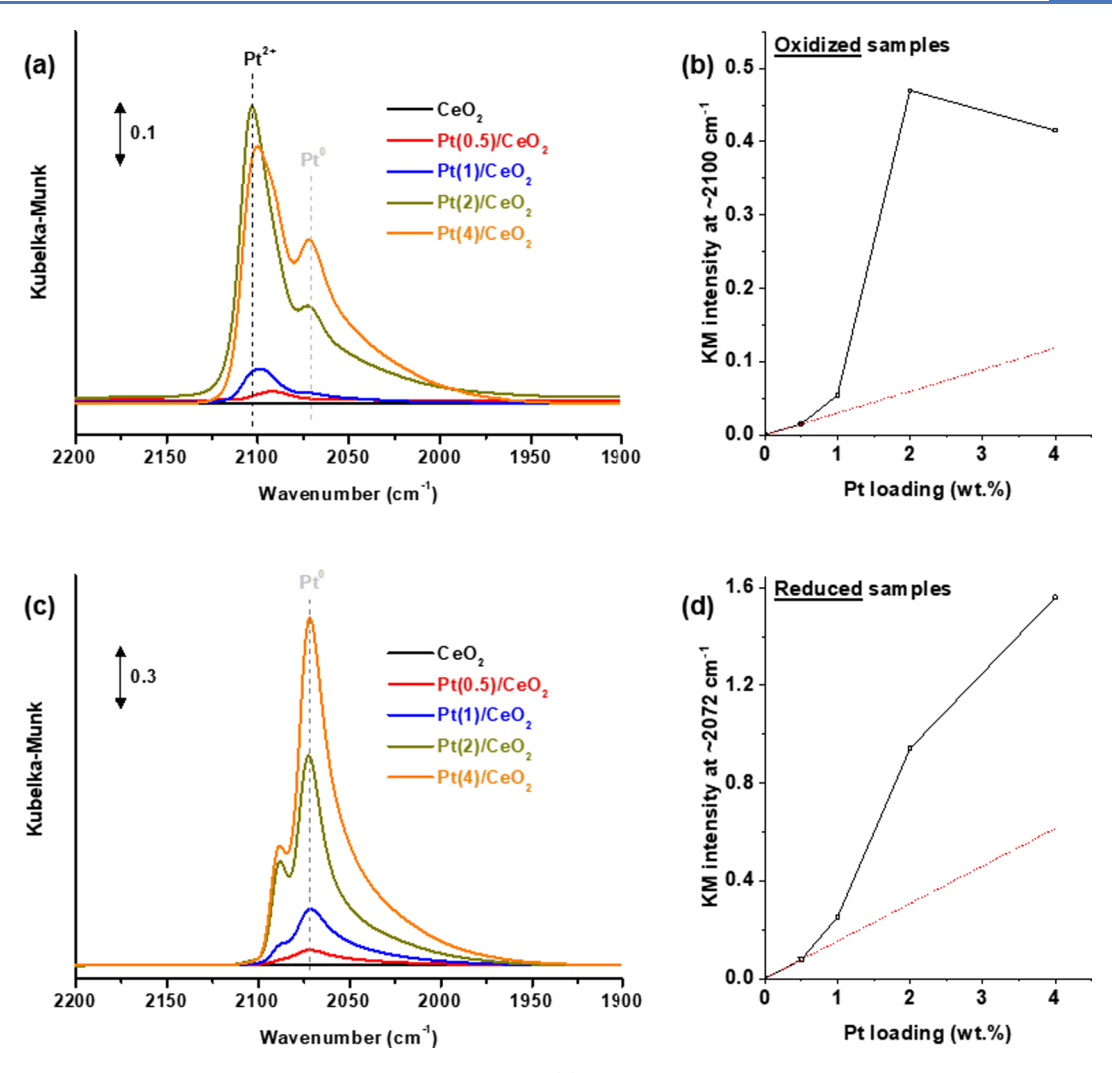


Figure 1. Preparation of Pt/CeO_2 catalysts with varying Pt nuclearity. (a) In situ CO-DRIFTS spectra of CeO_2 and Pt/CeO_2 with different Pt loadings (0.5–4 wt %) collected after reaction with 10% O_2 at 400 °C for 1 h. (b) Kubelka–Munk (KM) intensity at ~2100 cm⁻¹ as a function of Pt loading from the spectra in (a). (c) In situ CO-DRIFTS spectra collected after reaction with 10% H_2 at 400 °C for 1 h. (d) KM intensity at 2072 cm⁻¹ as a function of Pt loading from the spectra in (c). The lines connecting the data points in (b) and (d) are not model fits but are drawn to guide the eye. The dotted lines in (b) and (d) indicate the deviation from linearity of the KM intensity with respect to Pt loading. Note that the error bars for the $Pt(0.5)/CeO_2$ sample are included in (b) and (d) but not visible due to their small size (the KM values are 0.015 \pm 0.007 for the oxidized sample and 0.077 \pm 0.008 for the reduced sample). These KM values represent the standard deviation across three independently prepared batches.

2.2.6. CO Chemisorption. CO chemisorption measurements were conducted using a BELCAT II apparatus (MicrotracBEL, Japan) equipped with a thermal conductivity detector (TCD) for cryogenic operation. At room temperature, CO can chemisorb not only on Pt sites but also on CeO2, leading to the formation of various carbonaceous surface species. To suppress CO adsorption on CeO2 and selectively chemisorb CO on Pt, pulsed CO chemisorption was performed at -78 °C, assuming a stoichiometric CO-to-Pt ratio of 1.0.²⁹ Catalyst samples (0.05 g) were pretreated in situ with 5% H₂/Ar at 400 °C for 30 min, followed by He purging for 30 min. After cooling the system to -78 °C, successive pulses of 5% CO/He were introduced until saturation was achieved. Although CO adsorption on CeO₂ is significantly suppressed at -78 °C, a small amount of residual chemisorption still occurs. To correct for this background, we measured CO uptake on pure CeO2 under the same conditions. CO chemisorption was evaluated following two pretreatments: (i) oxidative pretreatment in 20% O₂ at 500 °C for 1 h, and (ii) reductive pretreatment in 5%

 $\rm H_2/Ar$ at 500 °C for 30 min. The amounts of CO chemisorbed on pure CeO₂ after these treatments were 9.1 μ mol/g and 13.1 μ mol/g, respectively. For analysis, we subtracted the average of these two values (11.1 μ mol/g) from the total CO uptake on Pt/CeO₂ to estimate the amount of CO chemisorbed specifically on Pt sites.

2.3. CO Oxidation Activity Evaluation. CO oxidation reactions were carried out in a fixed-bed reactor at atmospheric pressure using 10 or 15 mg of Pt/CeO₂ catalysts, diluted with appropriate amounts of pure CeO₂ depending on the specific experimental conditions. To evaluate the catalytic activity of Pt/CeO₂ samples with different nominal Pt loadings (0.5, 1, 2, and 4 wt %) while maintaining the same total amount of Pt, each catalyst was diluted with pure CeO₂ to match the Pt content. For example, Pt(4)/CeO₂ was mixed with pure CeO₂ at a mass ratio of 1:7 to match the Pt mass (0.075 mg Pt) of the Pt(0.5)/CeO₂ sample. In a separate set of experiments, the Pt(2)/CeO₂ catalyst was mixed with varying amounts of pure CeO₂ (mass ratios ranging from 0 to 6) to study the effect of

dilution while keeping the mass of Pt(2)/CeO₂ constant at 10 mg, thereby maintaining a constant total number of Pt atoms. All catalyst mixtures were prepared by physically mixing Pt/CeO₂ with pure CeO₂ powders using a vortex mixer, followed by sieving to obtain particles within the 150–180 μ m size range. The resulting mixtures were further diluted with inert α -Al₂O₃ (150–180 μ m) to dissipate heat generated during the reaction. We also confirmed that sieving the Pt/CeO₂ catalysts to a particle size of 150–180 μ m and mixing them with commercially available α -Al₂O₃ (150–180 μ m) effectively maintained a consistent flow rate across all experimental conditions, ensuring that the addition of excess CeO₂ during dilution did not result in any pressure drop within the reactor.

For the catalytic reaction, a gas mixture containing 1% CO and 10% O2, balanced with N2 to a total flow rate of 200 mL/ min, was used. Two distinct pretreatment conditions were applied: (i) to investigate the catalytic activity of the oxidized surface, the catalyst was treated in 10% O₂/N₂ at 400 °C for 1 h, followed by cooling to 40 $^{\circ}$ C under an 10% O_2/N_2 atmosphere. (ii) To study the activity of the reduced surface, the catalyst was pretreated in 10% H_2/N_2 at 400 °C for 1 h, cooled to 40 °C under H₂, and then purged with N₂ for 1 h. After pretreatment, the reaction was initiated by introducing the $CO/O_2/N_2$ reaction gas mixture, and the temperature was ramped from 40 to 400 °C at a rate of 2 °C/min. Data points for kinetic analysis were extracted from the linear (kinetic) region of the light-off curves to calculate the apparent turnover frequency (TOF), defined as the number of CO₂ molecules produced (measured from gas-cell IR) per second per total number of Pt atoms in the catalyst. Reaction orders for CO and O2 were determined at 50 °C. For O2 reaction order measurements, the partial pressure of O2 was varied between 19 and 76 Torr while maintaining CO at 7.6 Torr; for CO reaction order measurements, the CO partial pressure was varied from 0.76 to 7.6 Torr while O2 was held constant at 76 Torr. Kinetic data were collected after the reaction reached a steady state. Catalytic activity and product concentrations were monitored using a Nicolet iS50 FT-IR spectrometer (Thermo Fisher Scientific) equipped with a mercury cadmium telluride (MCT) detector.

3. RESULTS AND DISCUSSION

3.1. Preparation of Pt/CeO₂ Catalysts with Varying Pt Nuclearity. A series of Pt/CeO₂ catalysts were prepared with varying Pt loadings to investigate changes in Pt nuclearity. Pt was deposited onto CeO₂ nanoparticles (Rhodia, 8.6 nm average diameter, $142 \text{ m}^2/\text{g}$) using incipient wetness impregnation with a Pt(NH₃)₄(NO₃)₃ solution. Pt weight loadings ranged from 0.5 to 4 wt %, and the catalysts are denoted as Pt(X)/CeO₂.

To understand the changes in Pt nuclearity with Pt loading, and after oxidative and reductive pretreatments, in situ CO diffuse reflectance infrared Fourier transform spectroscopy (DRIFTS) spectra were collected for Pt/CeO₂ samples (Figure 1). Following oxidative pretreatment, a dominant peak appeared at ~2100 cm⁻¹, with a shoulder at ~2072 cm⁻¹ (Figure 1a). The assignment of the ~2100 cm⁻¹ band is controversial; some attribute it to CO bonded to Pt SAs, while others argue that Pt SAs on the CeO₂ surface cannot adsorb CO due to saturated coordination, instead assigning this band to CO bonded to Pt-oxide clusters. To clarify this, the intensity of the ~2100 cm⁻¹ band was plotted against Pt loading (Figure 1b). Interestingly, as Pt loading increased from

0.5 wt % to 1 and 2 wt %, the intensity of the \sim 2100 cm⁻¹ band increased nonlinearly. This suggests that in the samples studied, Pt SAs, which predominantly form at low Pt loadings, do not adsorb CO, whereas Pt-oxide clusters, which develop at higher Pt loadings, adsorb CO. Notably, the intensity of the ~2100 cm⁻¹ band increased sharply when Pt loading rose from 1 to 2 wt % (Figure 1b). It is hypothesized that defective sites capable of stabilizing Pt SAs become saturated at loadings above 1 wt %, leading to the formation of Pt-oxide clusters at higher loadings. In addition to the \sim 2100 cm⁻¹ band, a band at ~2072 cm⁻¹, assigned to CO linearly bound to undercoordinated Pt sites on Pt clusters, appeared as the Pt loading increased from 0.5 to 1 wt % (Figure 1a). The intensity of this band further increased as the Pt loading rose to 2 and 4 wt % (Figure 1a). Particularly, as the Pt loading increased from 2 to 4 wt %, the increase in the $\sim\!2072~\text{cm}^{-1}$ band intensity was accompanied by a decrease in the ~2100 cm⁻¹ band intensity (Figures 1a). X-ray photoelectron spectroscopy (XPS) did not reveal the presence of metallic Pt after oxidative pretreatment (Figure S1), suggesting that the metallic Pt clusters are formed due to the reduction of Pt-oxide clusters by CO. Additionally, a bridge-bonded CO band on Pt clusters at ~1840 cm⁻¹ was observed at higher Pt loadings (Figure S2), supporting the formation of Pt-oxide clusters (reduced by CO to form Pt clusters) at higher Pt loadings. That is, after oxidative treatment, Pt in Pt/CeO₂ primarily exists as SAs at low Pt loadings, but increasingly forms Pt-oxide clusters as the Pt loading increases.

To investigate changes in Pt nuclearity in Pt/CeO₂ samples after reductive pretreatment, in situ CO-DRIFTS spectra were collected following exposure to 10% H₂ at 400 °C for 1 h (Figure 1c). After this treatment, the CO band at \sim 2100 cm⁻¹ associated with Pt-oxide clusters, disappeared, while the CO band at ~2072 cm⁻¹, attributed to CO linearly bound to undercoordinated Pt sites on Pt clusters, became dominant. Additionally, CO linearly bound to well-coordinated Pt sites on Pt clusters, as well as Pt sites at the Pt cluster– CeO_2 interface, can contribute to the CO band at \sim 2090 cm^{-1,32,33} The intensity of the bridge-bonded CO band at ~1840 cm⁻¹ also increased with increasing Pt loading (Figure S3). Similar to the oxidized samples, the intensity of the CO-IR band at \sim 2072 cm $^{-1}$ in the reduced samples did not increase linearly with Pt loading (Figure 1d). If all Pt atoms were able to bind CO and Pt sintering was promoted at higher loadings, the intensity of the \sim 2072 cm⁻¹ band would be expected to show a concave downward trend with increasing Pt loading. However, the observed concave upward trend (Figure 1d) suggests that most of the Pt at low loadings remains atomically dispersed even after exposure to H₂ at 400 °C, rendering them unable to bind CO probe. It is likely that these Pt SAs are highly stable, with their coordination fully saturated by bonds with lattice oxygen atoms on the CeO2 surface, as reported in several previous studies. 30,34 Indeed, high-angle annular dark-field scanning transmission electron microscopy (HAADF-STEM) images confirmed that Pt SAs are mainly present in Pt(0.5)/ CeO₂ after treatment with H₂ at 400 °C (Figure S4), whereas Pt clusters are more prominent in Pt(4)/CeO₂ treated under the same condition (Figure S5).

It is worth to note that the spectra in Figure 1 are presented in Kubelka–Munk (KM) units rather than absorbance units. Previous studies have reported that when the relative reflectance ($R' = I/I_0$) exceeds 60% (corresponding to a KM intensity of approximately 0.13), the KM function more

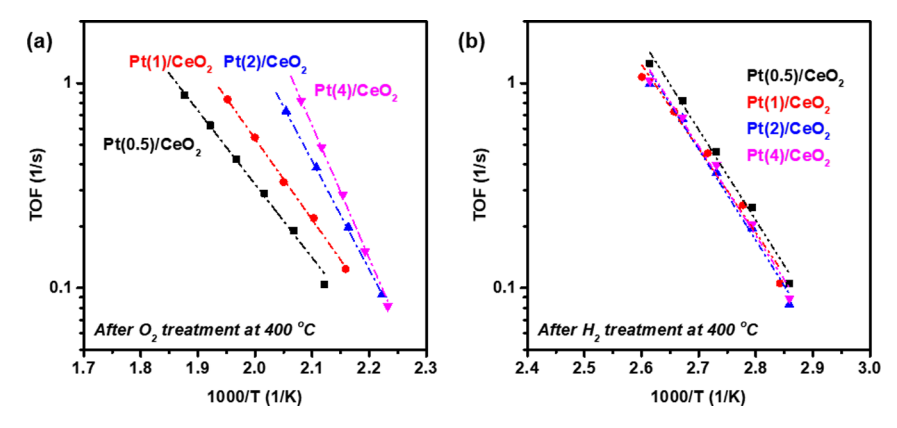


Figure 2. CO oxidation activity of Pt/CeO_2 catalysts with different distributions of Pt SAs and Pt clusters. The Arrhenius plots show the temperature dependence of CO oxidation activity for Pt/CeO_2 catalysts, following in situ pretreatment with (a) 10% O_2 at 400 °C for 1 h and (b) 10% O_2 at 400 °C for 1 h. The corresponding turnover frequency (TOF) versus temperature plots for (a) and (b) are provided in Figure S9. The TOF was calculated by determining the number of O_2 molecules generated per second, normalized to the total number of Pt atoms that are present in the catalyst. In these experiments, the total number of Pt atoms in each catalyst was kept constant by diluting O_2 catalysts with pure O_3 in appropriate mass ratios (e.g., O_3)/ O_3 and O_4 in a mass ratio of 1:7 to match the Pt mass of the O_3 / O_4 catalyst). Here, the total mass of the catalyst mixture in each experiment was fixed at 0.015 g. For the catalytic reaction, a gas mixture of 1% O_3 0 balanced with O_4 1 was flowed at a total rate of 200 mL/min. The apparent activation energy (O_4 1) for O_4 2 oxidation, estimated from the slope of the Arrhenius plot, is summarized in Table S1.

accurately represents the surface concentration of adsorbates on Pt/CeO₂.35 Conversely, when the relative reflectance is below 60%, absorbance provides a better linear correlation with the adsorbate surface concentration.³⁵ In Figure 1, the spectra for the reduced Pt/CeO₂ samples show KM intensities greater than 0.13, except for Pt(0.5)/CeO₂, where the KM intensity is 0.07. For comparison, the KM intensity for the reduced Pt(1)/CeO₂ is 0.25. As expected based on this intensity range, comparisons between CO chemisorption data and both absorbance and KM-based IR intensities show that KM units more accurately represent the amount of CO chemisorbed on Pt for the reduced samples (Figures S6 and S7; see detailed discussion in Figures S6 and S7). In contrast, the oxidized Pt/CeO₂ samples with Pt loadings ≤1 wt % exhibit KM intensities lower than 0.13 (Figure 1b). Although some deviations may occur for samples with KM intensities <0.13, the same trend can still be observed in the IR spectra plotted in absorbance unit for the oxidized samples (Figure S8).

In summary, in the series of Pt/CeO_2 catalysts with different Pt loadings, (i) Pt remains primarily atomically dispersed at low loadings (e.g., 0.5 wt % in this study) after both oxidative and reductive pretreatment at 400 °C, and (ii) the formation of Pt-oxide or metallic Pt clusters is favored at higher Pt loadings.

3.2. CO Oxidation Activity of Pt/CeO₂ Catalysts with Different Distributions of Pt SAs and Pt Clusters. The CO oxidation activity of Pt/CeO₂ catalysts is known to be highly dependent on the nuclearity of Pt species. Previous studies have shown that Pt SAs on CeO₂ surface exhibit lower activity than Pt clusters. However, this comparison typically assumes that Pt itself serves as the primary active site for the reaction, with limited exploration of the catalytic role played by CeO₂ surfaces distant from Pt sites.

To further investigate the contribution of these distant CeO₂ surfaces, we evaluated the CO oxidation activity of Pt/CeO₂ catalysts with varying Pt nuclearity, alongside an excess of CeO₂ surfaces, following oxidative or reductive pretreatments (Figure 2). The total Pt loading was kept constant at 0.5 wt % by diluting Pt/CeO₂ catalysts of different Pt concentrations with pure CeO₂. Note that the maximum Pt surface coverage

in $Pt(0.5)/CeO_2$ is less than 1% (Figure S10). Hence, this approach ensures a low Pt-to- CeO_2 site ratio, allowing us to specifically examine the catalytic influence of distant CeO_2 surfaces. The kinetics of the CO oxidation reaction were then measured under kinetically controlled condition (Figure S11).

After oxidative pretreatment at 400 °C, Pt/CeO₂ catalysts with Pt-oxide clusters exhibited significantly higher CO oxidation activity compared to those predominantly containing Pt SAs (Figure 2a). The activity increased with the proportion of Pt-oxide clusters, from Pt(0.5)/CeO₂ to Pt(4)/CeO₂. While the exact size and dispersion of the Pt-oxide clusters remain unknown, the results clearly indicate that Pt-oxide clusters are more effective for CO oxidation than Pt SAs, which aligns well with the previous findings. ^{20,30}

After reductive pretreatment at 400 °C, the CO oxidation activity of Pt/CeO₂ catalysts increased significantly (Figure 2a vs Figure 2b), consistent with previous reports. 22,30 Interestingly, unlike the behavior observed after oxidative pretreatment, the CO oxidation activities of Pt/CeO2 catalysts with varying distributions of Pt SAs and clusters were nearly identical following reductive pretreatment with 10% H₂ at 400 °C (Figure 2b). This questions several previous studies, which have reported that Pt clusters exhibit higher CO oxidation activity than Pt SAs, due to the weak CO binding on Pt SA $(E_{\rm ad.} \sim 0.04 \text{ eV})$. Interestingly, a similar phenomenon where the CO oxidation activity becomes independent of the Pt nuclearities after reductive pretreatment was reported recently, although detailed mechanistic explanation remains to be further explored.²² We hypothesize that the similar catalytic activity observed for Pt/CeO₂ catalysts with different distribution of Pt SAs and Pt clusters (Figure 2b) is attributed to the experimental condition used in our study, where an excess of CeO₂ is used relative to Pt.

To test this hypothesis, we mixed Pt(2)/CeO₂ with pure CeO₂ at varying mass ratios (pure CeO₂ to Pt(2)/CeO₂ from 0 to 6), while keeping the total amount of Pt(2)/CeO₂ in the mixture constant. This ensured that while the quantity and structure of Pt remained unchanged, the amount of pure CeO₂ in the mixture was varied. We also confirmed that the addition of CeO₂ did not affect the volumetric flow rate, which

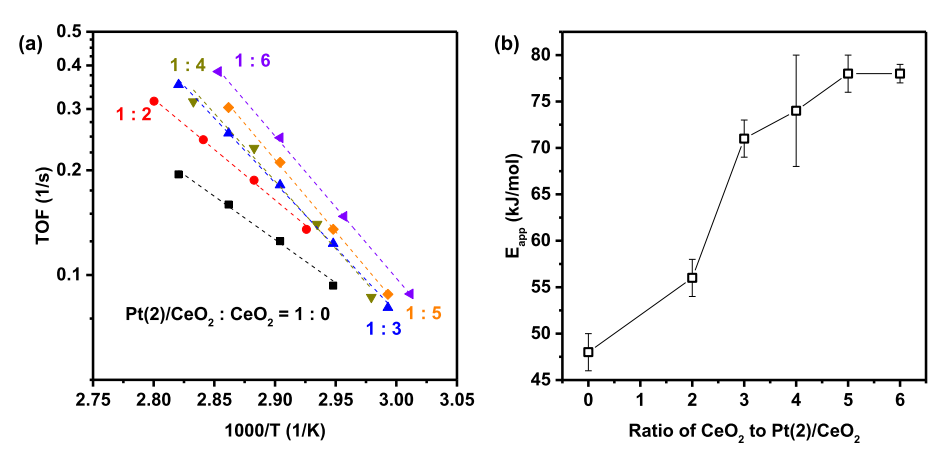


Figure 3. Influence of distant oxide surfaces on CO oxidation activity of Pt/CeO_2 catalysts. (a) Arrhenius plots showing the temperature dependence of CO oxidation activity for $Pt(2)/CeO_2$ catalysts mixed with pure CeO_2 in different mass ratios, following in situ reduction with 10% H_2 at 400 °C for 1 h. The corresponding TOF versus temperature plots for (a) are provided in Figure S14. The TOF was calculated by determining the number of CO_2 molecules generated per second, normalized to the total number of Pt atoms in the catalyst. In this experiment, the mass of $Pt(2)/CeO_2$ is fixed at 0.010 g to ensure a constant Pt content across samples. Also, the addition of CeO_2 did not alter the volumetric flow rate, which remained constant at 200 mL/min, confirming negligible pressure drop across the reactor. Reactions were carried out using a gas mixture of 1% CO and 10% O_2 (balanced with O_2) at a total flow rate of 200 mL/min. (b) Apparent activation energy (E_{app}) of CO oxidation for O_2 mixed with pure O_2 in different mass ratios plotted as a function of the mixing ratio of O_2 to O_2 . The error bars in (b) represent the standard error of the linear fits. See Table 1 for a summary of the kinetic parameters. The lines connecting the data points in (b) are not model fits but drawn to guide the eye.

remained constant at 200 mL/min, indicating negligible pressure drop. Note that pure CeO_2 exhibits negligible activity within the temperature range studied (Figure S12). If the CeO_2 particles were merely functioning as a diluent, the CO oxidation activity of these mixtures should be the same. However, we observed that the CO oxidation activity of $Pt(2)/CeO_2$ increased as more CeO_2 was added (Figure 3a). Furthermore, we observed that the CO oxidation activity of Pt/CeO_2 converged with similar apparent activation energy (E_{app}) when the dilution ratio of CeO_2 to $Pt(2)/CeO_2$ exceeded 4 (Figure 3b and Table 1). Here, the increase in the reaction rate for CO oxidation with the addition of pure CeO_2 is accompanied by a rise in E_{app} (Figure 3b), the

Table 1. Kinetic Parameters for the CO Oxidation Reaction Using Pt/CeO₂ Catalysts Mixed with Pure CeO₂ in Varying Mass Ratios^a

catalyst	$E_{\rm app}$ (kJ/mol)	ΔH^{\ddagger} (kJ/mol)	ΔS^{\ddagger} (J/mol·K)
$Pt(2)/CeO_2:CeO_2 = 1:0$	48 ± 2	45 ± 2	-111 ± 7
$Pt(2)/CeO_2:CeO_2 = 1:2$	56 ± 2	53 ± 2	-86 ± 5
$Pt(2)/CeO_2:CeO_2 = 1:3$	71 ± 2	68 ± 2	-42 ± 5
$Pt(2)/CeO_2:CeO_2 = 1:4$	74 ± 6	71 ± 6	-33 ± 18
$Pt(2)/CeO_2:CeO_2 = 1:5$	78 ± 2	76 ± 2	-17 ± 5
$Pt(2)/CeO_2:CeO_2 = 1:6$	78 ± 1	75 ± 1	-19 ± 4

"Apparent activation energy $(E_{\rm app})$ is determined from the Arrhenius plots (Figure 3a), while activation enthalpy (ΔH^{\ddagger}) and entropy (ΔS^{\ddagger}) are derived from the Eyring plots (Figures S15 and S16). Note that the quantity of Pt/CeO₂ used in the experiments was consistently 0.01 g, with the mass of CeO₂ varied from 0 to 0.06 g. Prior to reaction, the catalyst was treated with 10% H₂ at 400 °C for 1 h. The kinetic parameters were extracted from the kinetic regions (Figure S11). Note that the kinetics parameters for Pt(2)/CeO₂:CeO₂ = 1:5 and 1:6 show no significant difference within experimental uncertainty. A two-sample *t*-test confirms that they are statistically indistinguishable at 95% confidence, suggesting that $E_{\rm app}$, ΔH^{\ddagger} , and ΔS^{\ddagger} reach a plateau at dilution rations beyond 5.

underlying reason for which will be discussed later in Figure 4. Also, control experiments showed that the addition of CeO₂ to

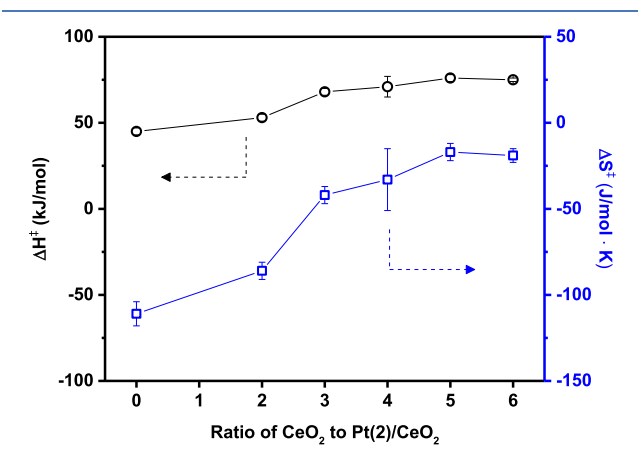


Figure 4. Influence of distant oxide surfaces on the CO oxidation kinetics of Pt/CeO_2 catalysts. The activation enthalpy (ΔH^{\ddagger}) and activation entropy (ΔS^{\ddagger}) of CO oxidation for Pt/CeO_2 catalysts mixed with pure CeO_2 in different mass ratios, estimated from the Eyring plots in Figure S16, plotted as a function of the mixing ratio of pure CeO_2 to $Pt(2)/CeO_2$. The error bars in the figure represent the standard error of the linear fits from the Eyring plots. See Table 1 for a summary of the kinetic parameters. The lines connecting the data points are not model fits but are drawn to guide the eye.

 $Pt(2)/CeO_2$ after oxidative pretreatment did not enhance the CO oxidation activity (Figure S13), supporting the conclusion that the observed activity enhancement after reductive pretreatment in Figure 3 arises from a chemical interaction rather than experimental artifacts. The mechanistic basis for this enhancement will be discussed in Figure 5 and the corresponding main text. These results suggest that, at high dilution ratios, the CO oxidation activity of Pt/CeO_2 is mainly governed by the catalytic function of CeO_2 surface. This observation indicates that the identical CO oxidation activity

ACS Catalysis pubs.acs.org/acscatalysis Research Article

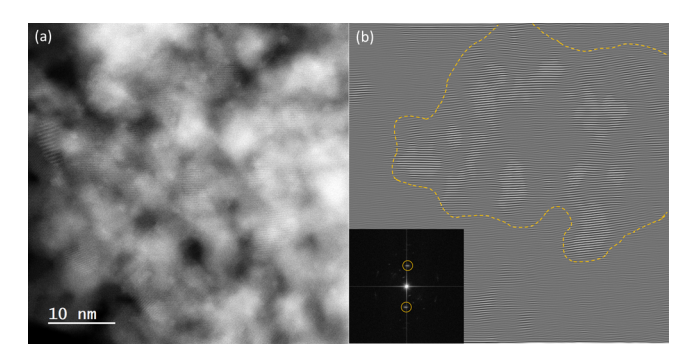


Figure 5. Aligned CeO_2 grain formation in H_2 -treated Pt/CeO_2 catalyst. (a) Representative HAADF-STEM image of the physical mixture of $Pt(2)/CeO_2$ and CeO_2 ($Pt(2)/CeO_2$: $CeO_2 = 1:6$), following reduction with 10% H_2 at 400 °C for 1 h. (b) Inverse FFTs showing CeO_2 domains with aligned grains, selected from the FFTs (orange circle). The FFTs of the image in (a) are displayed in the inset in (b).

of Pt/CeO₂ catalysts with different distribution of Pt SAs and clusters, as seen in Figure 2b, is likely due to the excess amount of CeO₂ surface present in each catalyst. Since pure CeO₂ exhibits negligible activity (Figure S12), Figure 3 suggests that the distant CeO₂ surface interacts with Pt to facilitate reaction.

To further elucidate the catalytic role of CeO2 surfaces, a deeper mechanistic understanding of the CO oxidation reaction is essential. The CO oxidation reaction over Pt/ CeO₂ catalysts is commonly explained by Mars-van Krevelen mechanism, where the CeO₂ surface near Pt provides labile oxygen to react with CO adsorbed on Pt (see Supplementary Discussion I for a discussion of the rationale drawn from previous studies for adopting this mechanism^{2,5,25,37-40}). According to this mechanism, the reaction begins with CO adsorption on Pt sites (eq 1). The adsorbed CO then reacts with O atoms on the CeO2 surface adjacent to Pt, producing CO_2 and creating oxygen vacancies (V_0) near Pt (eq 2). These V_0 s on the CeO₂ surface are replenished by gaseous O₂, completing the catalytic cycle (eq 4). Additionally, we introduced the rapid spillover of Vo across CeO2 surface as another elementary step (eq 3), given that $V_o s$ are known to be mobile on CeO_2 surface. This inclusion is supported by the significant increase in catalytic activity observed when CeO_2 was added to the physical mixture with $Pt(2)/CeO_2$ (Figure 3).

$$Pt + CO \rightleftharpoons Pt - CO$$
 (1)

$$Pt - CO + CeO_2 \rightleftharpoons Pt + CeO_{2-x} + CO_2$$
 (2)

$$CeO_{2-x} + CeO_2' \rightleftharpoons CeO_2 + CeO_{2-x}'$$
(3)

$$CeO'_{2-x} + \frac{1}{2}O_2 \rightleftharpoons CeO'_2 \tag{4}$$

Here, note that CeO_2 and CeO_2' refer to the CeO_2 surface sites near and distant from Pt, respectively. For the CO oxidation rate of Pt/CeO_2 to be independent of the different distribution of Pt SAs vs Pt clusters, eq 4 should represent the RLS. The scenarios where other reaction steps serve as the RLS are analyzed in Supplementary Discussion II, which demonstrates that in those cases, the rate is proportional to the Pt sites for CO activation. Assuming that eq 4, the replenishment of V_o , is the RLS, the CO oxidation rate can be described by eq 5 (see Supplementary Discussion II for detailed derivation).

$$r = \frac{k_4 K_1 K_2 K_3 P_{\text{CO}} \sqrt{P_{\text{O}_2}}}{K_1 K_2 K_3 P_{\text{CO}} + P_{\text{CO}_2}} \times [\text{CeO}_2']$$
(5)

Here, $P_{\rm CO}$, $P_{\rm O,2}$ and $P_{\rm CO2}$ denote the partial pressures of CO, O_2 , and CO_2 , respectively. K_1 , K_2 , and K_3 are the equilibrium constants for eqs 1, 2, and 3, respectively, and k_4 is the rate constant for eq 4. Given that the CO oxidation kinetics were evaluated at a low CO conversion (<15%, Figure S11), we can assume that $P_{\rm CO_2}$ is negligible ($P_{\rm CO_2} \sim 0$). Then, eq 5 simplifies to eq 6 as follows:

$$r = k_4 \sqrt{P_{O_2}} [CeO_2'] \tag{6}$$

Eq 6 shows that the reaction rate is insensitive to Pt structure and is instead proportional to the available CeO_2 surface sites distant from Pt, which is consistent with our observations in Figures 2 and 3. Therefore, under our experimental condition, the RLS is the replenishment of V_o by O_2 at CeO_2 surface sites away from Pt. This conclusion is further supported by the reaction order measurements over $Pt(2)/CeO_2$ diluted with pure CeO_2 at a 1 to 6 mass ratio, which revealed a reaction order of 0 with respect to CO and \sim 0.5 with respect to O_2 , in line with the rate expression in eq 6 (Figure S15).

Altogether, the kinetic analysis, combined with the observations in Figures 2 and 3, suggests that the CeO₂ surface sites, when physically mixed with Pt/CeO₂, can play a dominant role in the CO oxidation reaction. This explains the observed insensitivity of Pt/CeO2 catalysts to Pt structures in CO oxidation reaction when an abundance of CeO2 is present relative to Pt sites (Figure 2b). However, while the catalytic role of CeO₂ surface sites distant from Pt appears evident, it remains unclear why the reaction rate converges as the number of CeO₂ surface sites increases (Figure 3b). This convergence in reaction rate implies that the catalytic contribution of CeO2 surface sites is limited by certain constraints. Understanding these constraints can be crucial to establishing the structure-function relationship for Pt/CeO₂ catalysts, ultimately enabling more efficient use of expensive Pt by leveraging the catalytic potential of CeO₂ surface sites.

3.3. Entropic Contribution of Aligned Distant CeO₂ **Surface Sites in CO Oxidation.** In Figure 3, we observed that the increase in the reaction rate for CO oxidation with the addition of pure CeO_2 to $Pt(2)/CeO_2$ is accompanied by a corresponding rise in E_{app} . This suggests that the catalytic effect of CeO_2 may stem from entropic rather than enthalpic contributions. That is, CeO_2 may enhance the CO oxidation activity of Pt/CeO_2 by facilitating the formation of less constrained transition states, likely through the provision of labile oxygen atoms to the CO bound to Pt, rather than by lowering the energy barrier of the RLS.

To differentiate the enthalpic and entropic contributions of CeO₂ surfaces distant from Pt to the CO oxidation kinetics, the activation enthalpy (ΔH^{\ddagger}) and activation entropy (ΔS^{\ddagger}) for CO oxidation on Pt/CeO₂ catalysts mixed with varying amounts of pure CeO₂ were estimated using Eyring plots (Figure S16). Notably, both ΔH^{\ddagger} and ΔS^{\ddagger} for CO oxidation increased as the amount of CeO₂ in the Pt(2)/CeO₂ mixture was raised (Figure 4 and Table 1). Specifically, as the CeO₂-to-Pt(2)/CeO₂ mass ratio increased from 0 to 6, ΔH^{\ddagger} rose from 45 to 75 kJ/mol, while ΔS^{\ddagger} increased from -111 to -19 J/mol·K.

ACS Catalysis pubs.acs.org/acscatalysis Research Article

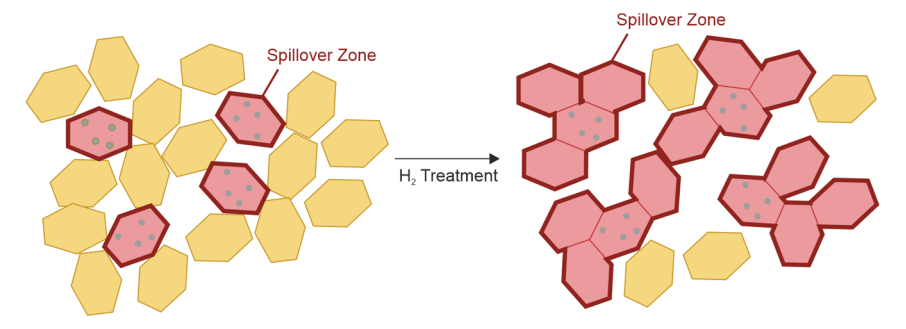


Figure 6. Schematic illustration of the O-spillover zone formation following H₂ treatment on Pt/CeO₂.

The increase in ΔH^{\ddagger} upon the addition of CeO₂ suggests that incorporating CeO₂ raises the energy barrier for the RLS, the replenishment of Vo on CeO2 surfaces by gaseous O2 (eq 4). It is well established that when gaseous O₂ adsorbs onto the Vos of CeO2, it forms peroxo or superoxo species. 41,42 The cleavage of the O-O bond requires a relatively high energy input, ranging from 29 to 175 kJ/mol, depending on the local coordination and detailed mechanisms involved in this process.^{26,43} Although further study is required to fully elucidate the mechanisms that activate O2 on CeO2 surfaces at varying proximities to Pt, it can be hypothesized that Pt may facilitate O₂ dissociation and promote oxygen spillover, similar to how it promotes H₂ dissociation and H-spillover. ^{6,7,44,45} However, as the CeO₂-to-Pt ratio increases, it is likely that Pt's influence on O2 activation diminishes, resulting in direct O2 activation on CeO_{2-x} surfaces. This explains the observed increase in ΔH^{\ddagger} as the amount of CeO₂ in the Pt(2)/CeO₂ mixture increases.

Although the increase in ΔH^{\ddagger} with the addition of more ${\rm CeO_2}$ to ${\rm Pt(2)/CeO_2}$ is unfavorable for the CO oxidation reaction, the rise in ΔS^{\ddagger} arising from the ${\rm CeO_2}$ addition more than compensates for the increase in ΔH^{\ddagger} (Figure 4). Consequently, the activation Gibbs free energy ($\Delta G^{\ddagger} = \Delta H^{\ddagger} - T\Delta S^{\ddagger}$) could decrease, leading to the enhanced catalytic activity despite the increase in $E_{\rm app}$ (Figure S17). Since the RLS for CO oxidation is the replenishment of ${\rm V_o}$ on ${\rm CeO_2}$ surfaces distant from Pt by gaseous ${\rm O_2}$ (eq 4), it is likely that the ${\rm O_2}$ activated on these ${\rm CeO_2}$ surfaces is being supplied to Pt sites. The increased availability of labile oxygen atoms around Pt may introduce additional configurational entropy to the transition state of CO reacting with oxygen atoms, boosting CO oxidation activity, as indicated by the increase in ΔS^{\ddagger} .

While kinetic analysis indicates that CeO_2 surface sites distant from Pt can enhance CO oxidation by supplying oxygen to Pt, it is essential to recognize the limitations of this promotional effect. As shown in Figure 4, the increase in ΔS^{\ddagger} plateaus when the CeO_2 -to-Pt(2)/CeO₂ mass ratio exceeds 4. This suggests that beyond a certain ratio, CeO_2 surface is no longer able to effectively deliver reactive oxygen to Pt.

To evaluate the limitations of adding additional CeO_2 to Pt/CeO_2 catalysts in enhancing the reaction rate, it is essential to first clarify the conditions under which this promotional effect occurs. Figure 2b shows that, following reductive pretreatment, CO oxidation activity becomes insensitive to the distribution of Pt present as SAs versus clusters. In contrast, after oxidative pretreatment, CO oxidation activity is sensitive to this distribution, with the catalysts containing clusters demonstrating higher activity (Figure 2a). Furthermore, the addition of pure CeO_2 to $Pt(2)/CeO_2$ does not improve the CO oxidation activity after oxidative pretreatment (Figure S13), indicating

that the reductive pretreatment is necessary for distant CeO_2 surfaces to promote CO oxidation reaction via O-spillover. This raises the question of what transformations occur in CeO_2 during reductive treatment and how these changes impact O-spillover rate from CeO_2 to Pt.

After H₂ treatment at 400 °C, XRD indicates that CeO₂ particles in Pt(2)/CeO₂ did not aggregate into larger crystallites (Figure S18). Interestingly, Fast Fourier transforms (FFTs) of the STEM image in Figure 5a for the physical mixture of Pt(2)/CeO₂ and pure CeO₂ in a 1 to 6 mass ratio suggest that the individual CeO2 particles share similar lattice orientations after the reductive pretreatment with H₂ at 400 °C (inset in Figure 5b). Typically, STEM images of randomly oriented particles exhibit ring-like diffraction patterns due to various crystal planes of randomly oriented particles (Figure S19). In contrast, oriented particles produce simpler diffraction patterns within a similar number of CeO₂ particles in the samesized field of view (Figures 5 and S20). This observation aligns with previous reports that the number of diffraction patterns for Pt/CeO₂ particles decreases following in situ H₂ reactions at 400 °C. 44 Moreover, inverse FFTs, which highlight selected CeO₂ domains (Figure 5b), reveal that the domain size of aligned CeO₂ grains is significantly larger than the average individual CeO2 particle size estimated from XRD pattern (\sim 60 vs \sim 10 nm). These results show that CeO₂ particles in Pt/CeO₂ form an oriented attachment state, a presintering stage where oxide nanoparticles align before aggregating into larger oxide particles. 44,46-50

When H₂ reacts with CeO₂ surface, reduction occurs at temperatures above 350 °C, leading to the formation of Vo. Due to the high surface energy of the reduced CeO₂ surfaces, these surfaces would energetically favor the formation of aligned grains, achieving a presintering state. 44,46-50 In situ TEM studies have demonstrated that this oriented attachment can occur at a much lower temperature under a reductive atmosphere (5% H₂) compared to an oxidative atmosphere (20% O_2), as the driving force for V_0 formation is much lower in the presence of oxygen.⁴⁴ Moreover, the presence of Pt on the CeO₂ surface can further promote V_o formation. Previous studies have demonstrated that the mechanism of H2 activation differs between Pt/CeO2 and CeO2: on bare CeO₂, H₂ tends to dissociate heterolytically, producing one surface hydroxyl (-OH) group and one Ce-H species. 44,45,51 These intermediates must subsequently convert into homolytic products in order to form H₂O and V₀. In contrast, when Pt is present, it enables direct homolytic dissociation of H2 into two -OH species, thereby bypassing the conversion step and facilitating more efficient V_o formation. 44,45 Hence, the presence of Pt is expected to enhance the formation of aligned

 CeO_2 grains under H_2 by promoting V_o formation and lowering the energy barrier for oriented attachment.

An interesting feature of the aligned CeO₂ grains is that the rate of H-spillover is significantly faster across the aligned CeO₂ grains compared to the nonaligned CeO₂ grains.⁴⁴ Although a detailed investigation of the O-spillover mechanism, and the effect of lattice alignment on O-spillover, is beyond the scope of this study, the similarity in the chemistries of H-spillover and O-spillover on CeO2 surface suggests that O-spillover may also be promoted across the aligned CeO₂ grains. 28,52 After H₂ pretreatment, facile O-spillover likely occurs from distant CeO2 surfaces to Pt, facilitating the CO oxidation reaction. However, this O-spillover would occur effective only within the aligned spillover zones, as schematically represented in Figure 6. This mechanism explains why the addition of CeO2 to Pt/CeO2 promotes CO oxidation only after reductive treatment, as the alignment of CeO2 domains necessary for efficient O-spillover occurs exclusively following reduction. It also accounts for the limited extent of the promotional effect of CeO₂ on reactivity. The inverse FFTs in Figure 5b reveal that the size of CeO₂ domain with aligned grains is ~60 nm, suggesting a limit to the growth of these aligned regions. While aligned CeO₂ grains may effectively supply labile O to Pt, CeO₂ grains outside these domains may contribute minimally to the reaction.

It is important to emphasize that the reaction mechanisms described in eqs 1-6, along with the discussion on CeO₂ particle alignment for promoting O-spillover, suggest that the catalytic activity of Pt/CeO₂ is influenced by the concentration of CeO₂ surface sites capable of supplying active O to Pt sites (referred to as CeO2' in eq 4). For the optimal activity, the lattice of these CeO2' particles should be aligned, and the CeO2' domain should encompass active Pt sites for CO activation (eq 1). In other words, if the dispersion of Pt over the CeO₂ particles is too low, the formation of aligned CeO₂ particles containing Pt sites would diminish, thereby reducing the reaction rate due to a lower concentration of CeO2' sites. Although the catalytic performance of Pt/CeO₂ catalyst is often attributed to Pt or Pt-CeO2 interface, our study highlights additional consideration when assessing the catalytic behavior of Pt/CeO₂.

Furthermore, the catalytic function of the metal–support interface can be modulated by interactions with remote oxide surfaces. In the system studied here, for instance, labile O supplied by distant CeO₂ domains can spillover to the Pt–CeO₂ interface, effectively increasing the chemical potential of reactive O species at the interface. This, in turn, may influence the local concentration of Ce³⁺ sites near Pt, potentially impacting reaction kinetics and the stabilization of intermediates in certain target reactions. Investigating the dynamic behavior of these interfacial species, particularly their response to remote oxide domains, through advanced operando spectroscopic techniques such as X-ray absorption spectroscopy (XAS) would provide valuable insights into the broader role of extended oxide surfaces in modulating catalytic reactivity.^{2,25}

The catalytic role of distant oxide surfaces in metal-oxide-supported heterogeneous catalysts, whether by directly participating in the RLS or by indirectly modulating the catalytic properties of metal—support interfaces through remote spillover chemistry, should be recognized as a broadly relevant and potentially universal phenomenon. A variety of spillover processes have been reported across different systems, including H-spillover over reducible oxides such as ${\rm CeO}_2^{11,44}$

and ${\rm TiO_2}_{,}^{7}$ proton spillover⁵³ over basic oxides like MgO and ${\rm Al_2O_3}$, O-spillover over ${\rm CeO_2}^{28}$ and ${\rm VO_x}^{54}$ and even the migration of larger molecules such as ${\rm C_2H_2}^{55}$ or benzene⁵⁶ across support surfaces. These observations suggest that remote oxide domains can actively contribute to catalytic reactions via spillover mechanisms. As such, the role of distant oxide surfaces warrants more rigorous attention in heterogeneous catalysis, where their contribution has often been overlooked. In some cases, the RLS may occur directly on these remote surfaces, as demonstrated in our ${\rm Pt/CeO_2}$ system, underscoring their potentially critical impact on overall catalytic performance.

Beyond the goal of optimizing the use of PGMs, our finding that the CeO₂ surfaces distant from Pt can greatly influence catalytic kinetics has broader implications for interpreting kinetic data and establishing structure-function relationships in catalytic reactions. Traditionally, the active sites in PGMsupported catalysts are defined as comprising PGM atoms in conjunction with adjacent oxide surfaces, and $E_{\rm app}$ is commonly used to identify active sites and differentiate the catalytic contributions of various species. However, in the case of CO oxidation over Pt/CeO_2 catalysts, E_{app} values span a wide range (~22 to ~120 kJ/mol) independent of Pt nuclearity (SAs vs nanoparticles) (Figure S21 and Table S2), resulting in conflicting interpretations across the literature. 2,4,5,20,24,25,39,40,57-65 While some studies suggest that Pt SAs on CeO_2 have lower E_{app} values than Pt nanoparticles, others report the opposite, making it difficult to draw a consistent structure-activity correlation. Our results add a new dimension to this complexity, demonstrating that E_{app} can vary significantly (from 48 to 78 kJ/mol) even when the Pt structure remains unchanged, solely due to the variations in the amount of CeO₂ surfaces that is spatially separated from Pt sites (Figure 3 and Table 1). This highlights the need to reconsider the role of distant CeO2 surface, which has often been overlooked, in oxidation reactions over Pt/CeO₂ catalysts. We believe that recognizing and integrating this perspective will deepen our understanding of structurefunction relationships and aid in the rational design of more efficient catalytic systems for a broad range of catalytic applications.

4. CONCLUSIONS

In this study, we have demonstrated that CeO₂ surfaces located several nanometers away from Pt can actively contribute to the CO oxidation reaction, challenging the common assumption that only PGMs and adjacent oxide surfaces participate in catalysis. Our findings show that oxygen spillover from distant CeO₂ surfaces plays a significant role in facilitating catalytic activity, especially as the CeO2 content in Pt/CeO2 catalyst increases. Kinetic analysis revealed that the RLS for CO oxidation in CeO₂-rich Pt/CeO₂ catalysts is oxygen activation over these distant CeO₂ surfaces, a process that becomes independent of the distribution of Pt existing as SAs or clusters beyond a certain CeO2 dilution threshold. Furthermore, the alignment of CeO₂ grains during reductive treatment is found to be important in promoting the oxygen spillover from distant CeO₂ to Pt, thereby enhancing the catalytic performance. These insights highlight the importance of considering distant oxide surfaces when establishing structure-function relationships in PGM-supported oxide catalysts, an aspect that has not been fully considered and could have a profound impact on the field. By accounting for the catalytic roles of distant surfaces, it

would be possible to better optimize catalyst design, particularly in applications where maximizing the efficiency of PGMs is critical. Our results provide new directions for the development of efficient catalysts, not only for CO oxidation but potentially for a wide range of thermo-catalytic and electrocatalytic reactions where oxide surface plays a key role.

ASSOCIATED CONTENT

3 Supporting Information

The Supporting Information is available free of charge at https://pubs.acs.org/doi/10.1021/acscatal.5c01564.

Additional CO oxidation reaction and characterizations (XP spectra, DRIFTS spectra, STEM images, XRD patterns, and N_2 adsorption/desorption isotherms) (PDF)

AUTHOR INFORMATION

Corresponding Authors

Jaeha Lee — School of Chemical Engineering and Applied Chemistry, Kyungpook National University, Daegu 41566, Republic of Korea; ⊚ orcid.org/0000-0001-6879-5012; Email: jaeha0913@knu.ac.kr

Do Heui Kim — School of Chemical and Biological Engineering, Institute of Chemical Processes, Seoul National University, Seoul 08826, Republic of Korea; orcid.org/ 0000-0003-3870-1606; Email: dohkim@snu.ac.kr

Authors

Eunwon Lee — School of Chemical and Biological Engineering, Institute of Chemical Processes, Seoul National University, Seoul 08826, Republic of Korea

Sungsu Kang — School of Chemical and Biological Engineering, Institute of Chemical Processes, Seoul National University, Seoul 08826, Republic of Korea

Arik Beck — Institute for Chemical Technology and Polymer Chemistry, Karlsruhe Institute of Technology, Karlsruhe 76131, Germany; ● orcid.org/0000-0001-5267-3141

Jungwon Park — School of Chemical and Biological
Engineering, Institute of Chemical Processes, Seoul National
University, Seoul 08826, Republic of Korea; Center for
Nanoparticle Research, Institute for Basic Science (IBS),
Seoul National University, Seoul 08826, Republic of Korea;
orcid.org/0000-0003-2927-4331

Complete contact information is available at: https://pubs.acs.org/10.1021/acscatal.5c01564

Notes

The authors declare no competing financial interest.

ACKNOWLEDGMENTS

This research was supported by the Basic Science Research Program and National R&D Program through the National Research Foundation of Korea (NRF) funded by the Ministry of Science, ICT & Future Planning (RS-2025-00519715 and 2022M3J2A1085551). This work is also partially supported by the National Research Foundation of Korea (NRF) grant funded by the Korea government (MOE) (No. 2120241415340, BK21 Program for Low-Carbon Advanced Materials Innovation).

REFERENCES

- (1) Cargnello, M.; Doan-Nguyen, V. V.; Gordon, T. R.; Diaz, R. E.; Stach, E. A.; Gorte, R. J.; Fornasiero, P.; Murray, C. B. Control of metal nanocrystal size reveals metal-support interface role for ceria catalysts. *Science* **2013**, *341* (6147), 771–773.
- (2) Kopelent, R.; van Bokhoven, J. A.; Szlachetko, J.; Edebeli, J.; Paun, C.; Nachtegaal, M.; Safonova, O. V. Catalytically active and spectator Ce³⁺ in ceria-supported metal catalysts. *Angew. Chem.* **2015**, 127 (30), 8852–8855.
- (3) Daelman, N.; Capdevila-Cortada, M.; López, N. Dynamic charge and oxidation state of Pt/CeO₂ single-atom catalysts. *Nat. Mater.* **2019**, *18* (11), 1215–1221.
- (4) Lu, Y.; Zhou, S.; Kuo, C.-T.; Kunwar, D.; Thompson, C.; Hoffman, A. S.; Boubnov, A.; Lin, S.; Datye, A. K.; Guo, H.; Karim, A. M. Unraveling the Intermediate Reaction Complexes and Critical Role of Support-Derived Oxygen Atoms in CO Oxidation on Single-Atom Pt/CeO₂. ACS Catal. 2021, 11 (14), 8701–8715.
- (5) Nie, L.; Mei, D.; Xiong, H.; Peng, B.; Ren, Z.; Pereira Hernández, X. I.; DeLaRiva, A.; Wang, M.; Engelhard, M. H.; Kovarik, L.; Datye, A. K.; Wang, Y. Activation of surface lattice oxygen in single-atom Pt/CeO₂ for low-temperature CO oxidation. *Science* **2017**, 358 (6369), 1419–1423.
- (6) Prins, R. Hydrogen Spillover. Facts and Fiction. Chem. Rev. 2012, 112 (5), 2714–2738.
- (7) Karim, W.; Spreafico, C.; Kleibert, A.; Gobrecht, J.; VandeVondele, J.; Ekinci, Y.; van Bokhoven, J. A. Catalyst support effects on hydrogen spillover. *Nature* **2017**, *541* (7635), 68–71.
- (8) Briggs, N. M.; Barrett, L.; Wegener, E. C.; Herrera, L. V.; Gomez, L. A.; Miller, J. T.; Crossley, S. P. Identification of active sites on supported metal catalysts with carbon nanotube hydrogen highways. *Nat. Commun.* **2018**, *9* (1), 3827.
- (9) Gomez, L. A.; Bababrik, R.; Komarneni, M. R.; Marlowe, J.; Salavati-fard, T.; D'Amico, A. D.; Wang, B.; Christopher, P.; Crossley, S. P. Selective reduction of carboxylic acids to aldehydes with promoted MoO₃ catalysts. *ACS Catal.* **2022**, *12* (11), 6313–6324.
- (10) Kim, H.; Yang, S.; Lim, Y. H.; Lee, J.; Ha, J.-M.; Kim, D. H. Enhancement in the metal efficiency of Ru/TiO_2 catalyst for guaiacol hydrogenation via hydrogen spillover in the liquid phase. *J. Catal.* **2022**, *410*, 93–102.
- (11) Beck, A.; Kazazis, D.; Ekinci, Y.; Li, X.; Müller Gubler, E. A.; Kleibert, A.; Willinger, M.-G.; Artiglia, L.; van Bokhoven, J. A. The extent of platinum-induced hydrogen spillover on cerium dioxide. *ACS Nano* **2023**, *17* (2), 1091–1099.
- (12) Chen, J.; Xiong, S.; Liu, H.; Shi, J.; Mi, J.; Liu, H.; Gong, Z.; Oliviero, L.; Maugé, F.; Li, J. Reverse oxygen spillover triggered by CO adsorption on Sn-doped Pt/TiO₂ for low-temperature CO oxidation. *Nat. Commun.* **2023**, *14* (1), 3477.
- (13) Mahdavi-Shakib, A.; Whittaker, T. N.; Yun, T. Y.; Sravan Kumar, K. B.; Rich, L. C.; Wang, S.; Rioux, R. M.; Grabow, L. C.; Chandler, B. D. The role of surface hydroxyls in the entropy-driven adsorption and spillover of H₂ on Au/TiO₂ catalysts. *Nat. Catal.* **2023**, *6* (8), 710–719.
- (14) Shun, K.; Mori, K.; Kidawara, T.; Ichikawa, S.; Yamashita, H. Heteroatom doping enables hydrogen spillover via H^+/e^- diffusion pathways on a non-reducible metal oxide. *Nat. Commun.* **2024**, *15* (1), 6403.
- (15) Xie, J.; Cheng, J.; Peng, J.; Zhang, J.; Wu, X.; Zhang, R.; Li, Z.; Li, C. A Tandem Catalysis for Isoindolinone Synthesis over Single-atom Pd/TiO₂ Catalyst. *Angew. Chem., Int. Ed.* **2024**, No. e202415203.
- (16) Khoobiar, S. Particle to Particle Migration of Hydrogen Atoms on Platinum—Alumina Catalysts from Particle to Neighboring Particles. *J. Phys. Chem.* **1964**, *68* (2), 411–412.
- (17) Weng, L.-T.; Delmon, B. Phase cooperation and remote control effects in selective oxidation catalysts. *Appl. Catal. A: Gen.* **1992**, *81* (2), 141–213.
- (18) Delmon, B.; Froment, G. F. Remote Control of Catalytic Sites by Spillover Species: A Chemical Reaction Engineering Approach. *Catal. Rev.* **1996**, 38 (1), 69–100.

- (19) Lee, J.; Ryou, Y.; Chan, X.; Kim, T. J.; Kim, D. H. How Pt Interacts with CeO₂ under the Reducing and Oxidizing Environments at Elevated Temperature: The Origin of Improved Thermal Stability of Pt/CeO₂ Compared to CeO₂. *J. Phys. Chem. C* **2016**, *120* (45), 25870–25879.
- (20) Pereira-Hernández, X. I.; DeLaRiva, A.; Muravev, V.; Kunwar, D.; Xiong, H.; Sudduth, B.; Engelhard, M.; Kovarik, L.; Hensen, E. J. M.; Wang, Y.; Datye, A. K. Tuning Pt-CeO₂ interactions by high-temperature vapor-phase synthesis for improved reducibility of lattice oxygen. *Nat. Commun.* **2019**, *10* (1), 1358.
- (21) Maurer, F.; Jelic, J.; Wang, J.; Gänzler, A.; Dolcet, P.; Wöll, C.; Wang, Y.; Studt, F.; Casapu, M.; Grunwaldt, J.-D. Tracking the formation, fate and consequence for catalytic activity of Pt single sites on CeO₂. *Nat. Catal.* **2020**, *3* (10), 824–833.
- (22) Maurer, F.; Beck, A.; Jelic, J.; Wang, W.; Mangold, S.; Stehle, M.; Wang, D.; Dolcet, P.; Gänzler, A. M.; Kübel, C.; Studt, F.; Casapu, M.; Grunwaldt, J.-D. Surface Noble Metal Concentration on Ceria as a Key Descriptor for Efficient Catalytic CO Oxidation. ACS Catal. 2022, 12 (4), 2473–2486.
- (23) Ding, C.; Gu, Q.; Yu, L.-J.; Zhang, S.; Zhang, Y.; Ma, Z.; Meng, Y.; Zhang, H.; Wang, T.; Wang, J.; Ma, L.; Li, G.; Yang, B.; Zhang, T. Reversible transformation and distribution determination of diverse Pt single-atom species. *J. Am. Chem. Soc.* **2023**, *145* (4), 2523–2531.
- (24) Fu, N.; Liang, X.; Wang, X.; Gan, T.; Ye, C.; Li, Z.; Liu, J.-C.; Li, Y. Controllable conversion of platinum nanoparticles to single atoms in Pt/CeO₂ by laser ablation for efficient CO oxidation. *J. Am. Chem. Soc.* **2023**, *145* (17), 9540–9547.
- (25) Kopelent, R.; Tereshchenko, A.; Guda, A.; Smolentsev, G.; Artiglia, L.; Sushkevich, V. L.; Bugaev, A.; Sadykov, I. I.; Baidya, T.; Bodnarchuk, M.; van Bokhoven, J. A.; Nachtegaal, M.; Safonova, O. V. Enhanced reducibility of the ceria—tin oxide solid solution modifies the CO oxidation mechanism at the platinum—oxide interface. *ACS Catal.* **2021**, *11* (15), 9435—9449.
- (26) Chen, H. T.; Chang, J. G.; Chen, H. L.; Ju, S. P. Identifying the O₂ diffusion and reduction mechanisms on CeO₂ electrolyte in solid oxide fuel cells: a DFT+ U study. *J. Comput. Chem.* **2009**, *30* (15), 2433–2442.
- (27) Lee, E.; Lee, J.; Hwang, S.; Kim, D. H. Role of CeO_2 in promoting the spillover in CO oxidation reaction over platinum nanoparticle-supported CeO_2 catalyst. *J. Catal.* **2023**, *417*, 421–431.
- (28) Vayssilov, G. N.; Lykhach, Y.; Migani, A.; Staudt, T.; Petrova, G. P.; Tsud, N.; Skála, T.; Bruix, A.; Illas, F.; Prince, K. C.; Matolin, V.; Neyman, K. M.; Libuda, J. Support nanostructure boosts oxygen transfer to catalytically active platinum nanoparticles. *Nat. Mater.* **2011**, *10* (4), 310–315.
- (29) Tanabe, T.; Nagai, Y.; Hirabayashi, T.; Takagi, N.; Dohmae, K.; Takahashi, N.; Matsumoto, S. i.; Shinjoh, H.; Kondo, J. N.; Schouten, J. C.; Brongersma, H. H. Low temperature CO pulse adsorption for the determination of Pt particle size in a Pt/cerium-based oxide catalyst. *Appl. Catal. A: Gen.* **2009**, *370* (1), 108–113.
- (30) Resasco, J.; DeRita, L.; Dai, S.; Chada, J. P.; Xu, M.; Yan, X.; Finzel, J.; Hanukovich, S.; Hoffman, A. S.; Graham, G. W.; Bare, S. R.; Pan, X.; Christopher, P. Uniformity is key in defining structure—function relationships for atomically dispersed metal catalysts: The case of Pt/CeO₂. J. Am. Chem. Soc. **2020**, 142 (1), 169–184.
- (31) Meunier, F. C. Relevance of IR Spectroscopy of Adsorbed CO for the Characterization of Heterogeneous Catalysts Containing Isolated Atoms. *J. Phys. Chem. C* **2021**, *125* (40), 21810–21823.
- (32) Happel, M.; Mysliveček, J.; Johánek, V.; Dvořák, F.; Stetsovych, O.; Lykhach, Y.; Matolín, V.; Libuda, J. Adsorption sites, metal-support interactions, and oxygen spillover identified by vibrational spectroscopy of adsorbed CO: A model study on Pt/ceria catalysts. *J. Catal.* **2012**, 289, 118–126.
- (33) Lee, J.; Shin, D.; Lee, E.; Li, C.; Kim, J. M.; Han, J. W.; Kim, D. H. Alleviating inhibitory effect of H₂ on low-temperature water-gas shift reaction activity of Pt/CeO₂ catalyst by forming CeO₂ nanopatches on Pt nano-particles. *Appl. Catal. B: Environ.* **2022**, 305, No. 121038.

- (34) Bruix, A.; Lykhach, Y.; Matolínová, I.; Neitzel, A.; Skála, T.; Tsud, N.; Vorokhta, M.; Stetsovych, V.; Ševčíková, K.; Mysliveček, J. Maximum noble-metal efficiency in catalytic materials: atomically dispersed surface platinum. *Angew. Chem., Int. Ed.* **2014**, 53 (39), 10525–10530.
- (35) Sirita, J.; Phanichphant, S.; Meunier, F. C. Quantitative analysis of adsorbate concentrations by diffuse reflectance FT-IR. *Anal. Chem.* **2007**, 79 (10), 3912–3918.
- (36) Liu, L.; Meira, D. M.; Arenal, R.; Concepcion, P.; Puga, A. V.; Corma, A. Determination of the evolution of heterogeneous single metal atoms and nanoclusters under reaction conditions: which are the working catalytic sites? *ACS Catal.* **2019**, *9* (12), 10626–10639.
- (37) Muravev, V.; Simons, J. F.; Parastaev, A.; Verheijen, M. A.; Struijs, J. J.; Kosinov, N.; Hensen, E. J. M. Operando spectroscopy unveils the catalytic role of different palladium oxidation states in CO oxidation on Pd/CeO₂ catalysts. *Angew. Chem., Int. Ed.* **2022**, *61* (23), No. e202200434.
- (38) Muravev, V.; Parastaev, A.; van den Bosch, Y.; Ligt, B.; Claes, N.; Bals, S.; Kosinov, N.; Hensen, E. J. M. Size of cerium dioxide support nanocrystals dictates reactivity of highly dispersed palladium catalysts. *Science* **2023**, 380 (6650), 1174–1179.
- (39) Wang, C.; Gu, X.-K.; Yan, H.; Lin, Y.; Li, J.; Liu, D.; Li, W.-X.; Lu, J. Water-mediated Mars-Van Krevelen mechanism for CO oxidation on ceria-supported single-atom Pt₁ catalyst. *ACS Catal.* **2017**, 7 (1), 887–891.
- (40) Lu, Y.; Thompson, C.; Kunwar, D.; Datye, A. K.; Karim, A. M. Origin of the high CO oxidation activity on CeO₂ supported Pt nanoparticles: weaker binding of CO or facile oxygen transfer from the support? *ChemCatChem.* **2020**, *12* (6), 1726–1733.
- (41) Choi, Y.; Abernathy, H.; Chen, H. T.; Lin, M.-C.; Liu, M. Characterization of O_2 – CeO_2 interactions using in situ Raman spectroscopy and first-principle calculations. *ChemPhysChem* **2006**, 7 (9), 1957–1963.
- (42) Yang, C.; Yu, X.; Heißler, S.; Weidler, P. G.; Nefedov, A.; Wang, Y.; Wöll, C.; Kropp, T.; Paier, J.; Sauer, J. O₂ activation on ceria catalysts—the importance of substrate crystallographic orientation. *Angew. Chem., Int. Ed.* **2017**, *56* (51), 16399–16404.
- (43) Wang, Y.-G.; Mei, D.; Li, J.; Rousseau, R. DFT+ U study on the localized electronic states and their potential role during H₂O dissociation and CO oxidation processes on CeO₂ (111) surface. *J. Phys. Chem. C* 2013, 117 (44), 23082–23089.
- (44) Lee, J.; Tieu, P.; Finzel, J.; Zang, W.; Yan, X.; Graham, G.; Pan, X.; Christopher, P. How Pt Influences H₂ Reactions on High Surface-Area Pt/CeO₂ Powder Catalyst Surfaces. *JACS Au* **2023**, 3 (8), 2299–2313.
- (45) Lee, J.; Christopher, P. Does H₂ Temperature-Programmed Reduction Always Probe Solid-State Redox Chemistry? The Case of Pt/CeO₂. Angew. Chem., Int. Ed. **2025**, 64 (2), No. e202414388.
- (46) Hojo, H.; Mizoguchi, T.; Ohta, H.; Findlay, S. D.; Shibata, N.; Yamamoto, T.; Ikuhara, Y. Atomic structure of a CeO₂ grain boundary: the role of oxygen vacancies. *Nano Lett.* **2010**, *10* (11), 4668–4672.
- (47) Bouala, G. N.; Clavier, N.; Lechelle, J.; Mesbah, A.; Dacheux, N.; Podor, R. In situ HT-ESEM study of crystallites growth within CeO₂ microspheres. *Ceram. Int.* **2015**, *41* (10), 14703–14711.
- (48) Nkou Bouala, G.; Clavier, N.; Martin, S.; Léchelle, J.; Favrichon, J.; Brau, H.; Dacheux, N.; Podor, R. From in situ HT-ESEM observations to simulation: how does polycrystallinity affects the sintering of CeO₂ microspheres? *J. Phys. Chem. C* **2016**, *120* (1), 386–395.
- (49) Feng, B.; Sugiyama, I.; Hojo, H.; Ohta, H.; Shibata, N.; Ikuhara, Y. Atomic structures and oxygen dynamics of CeO_2 grain boundaries. *Sci. Rep.* **2016**, 6 (1), 20288.
- (50) Lee, J.; Kang, S.; Lee, E.; Kang, M.; Sung, J.; Kim, T. J.; Christopher, P.; Park, J.; Kim, D. H. Aggregation of CeO₂ particles with aligned grains drives sintering of Pt single atoms in Pt/CeO₂ catalysts. *J. Mater. Chem. A* **2022**, *10* (13), 7029–7035.
- (51) Werner, K.; Weng, X.; Calaza, F.; Sterrer, M.; Kropp, T.; Paier, J.; Sauer, J.; Wilde, M.; Fukutani, K.; Shaikhutdinov, S.; Freund, H.-J.

- Toward an Understanding of Selective Alkyne Hydrogenation on Ceria: On the Impact of O Vacancies on H₂ Interaction with CeO₂(111). *J. Am. Chem. Soc.* **2017**, *139* (48), 17608–17616.
- (52) Lykhach, Y.; Staudt, T.; Vorokhta, M.; Skála, T.; Johánek, V.; Prince, K. C.; Matolín, V.; Libuda, J. Hydrogen spillover monitored by resonant photoemission spectroscopy. *J. Catal.* **2012**, 285 (1), 6–9.
- (53) Li, J.; Li, G.; Tsang, S. C. E. Heterogeneous Frustrated Lewis Pair Catalysts: Rational Structure Design and Mechanistic Elucidation Based on Intrinsic Properties of Supports. *Acc. Chem. Res.* **2025**, 8761–8771.
- (54) Al Abdulghani, A. J.; Kurumbail, U.; Dong, S.; Altvater, N. R.; Dorn, R. W.; Cendejas, M. C.; McDermott, W. P.; Agbi, T. O.; Queen, C. M.; Alvear, M.; Head, A. R.; Rossini, A. J.; Hermans, I. Preventing Loss of Selectivity during the Oxidative Dehydrogenation of Propane over Supported Vanadium Catalysts. *ACS Catal.* **2025**, *15*, 5557–5567.
- (55) Duan, X.; Zhao, Y.; Chou, H.-L.; Zuo, J.; Wang, R.; Jiao, W.; Fang, H.; Zheng, Y.; Lin, H.; Ye, L.; Yuan, Y. Reversible Spillover Wakens Reactivity of Dormant Modular Hydrochlorination Catalysts. *ACS Catal.* **2025**, *15* (5), 3913–3927.
- (56) Li, Z.; Meng, F.; Yang, X.; Qi, Y.; Qin, Y.; Zhang, B. J. The role of Mo single atoms and clusters in enhancing Pt catalyst for benzene hydrogenation: Distinguishing between benzene spillover and electronic effect. ACS Catal. 2024, 14 (7), 5016–5026.
- (57) Wang, W.; Li, D.; Yu, H.; Liu, C.; Tang, C.; Chen, J.; Lu, J.; Luo, M. Insights into different reaction behaviors of propane and CO oxidation over Pt/CeO₂ and Pt/Nb₂O₅: The crucial roles of support properties. *J. Phys. Chem. C* **2021**, *125* (35), 19301–19310.
- (58) Wang, Y.; Ma, J.; Wang, X.; Zhang, Z.; Zhao, J.; Yan, J.; Du, Y.; Zhang, H.; Ma, D. Complete CO Oxidation by O_2 and H_2O over Pt– $CeO_{2-\delta}/MgO$ Following Langmuir–Hinshelwood and Mars–van Krevelen Mechanisms, Respectively. *ACS Catal.* **2021**, *11* (19), 11820–11830.
- (59) Liu, H.-H.; Wang, Y.; Jia, A.-P.; Wang, S.-Y.; Luo, M.-F.; Lu, J.-Q. Oxygen vacancy promoted CO oxidation over Pt/CeO₂ catalysts: A reaction at Pt–CeO₂ interface. *Appl. Surf. Sci.* **2014**, *314*, 725–734.
- (60) An, K.; Alayoglu, S.; Musselwhite, N.; Plamthottam, S.; Melaet, G. r. M.; Lindeman, A. E.; Somorjai, G. A. Enhanced CO oxidation rates at the interface of mesoporous oxides and Pt nanoparticles. *J. Am. Chem. Soc.* **2013**, *135* (44), *16689*–16696.
- (61) Yoon, S.; Ha, H.; Kim, J.; Nam, E.; Yoo, M.; Jeong, B.; Kim, H. Y.; An, K. Influence of the Pt size and CeO₂ morphology at the Pt–CeO₂ interface in CO oxidation. *J. Mater. Chem. A* **2021**, 9 (46), 26381–26390.
- (62) Zhang, J.; Qin, X.; Chu, X.; Chen, M.; Chen, X.; Chen, J.; He, H.; Zhang, C. Tuning metal—support interaction of Pt-CeO₂ catalysts for enhanced oxidation reactivity. *Environ. Sci. Technol.* **2021**, *55* (24), 16687–16698.
- (63) Jones, J.; Xiong, H.; DeLaRiva, A. T.; Peterson, E. J.; Pham, H.; Challa, S. R.; Qi, G.; Oh, S.; Wiebenga, M. H.; Pereira Hernández, X. I. Thermally stable single-atom platinum-on-ceria catalysts via atom trapping. *Science* **2016**, 353 (6295), 150–154.
- (64) Chen, J.; Wanyan, Y.; Zeng, J.; Fang, H.; Li, Z.; Dong, Y.; Qin, R.; Wu, C.; Liu, D.; Wang, M. Surface engineering protocol to obtain an atomically dispersed Pt/CeO₂ catalyst with high activity and stability for CO oxidation. ACS Sustainable Chem. Eng. 2018, 6 (11), 14054–14062.
- (65) Wang, H.; Liu, J.-X.; Allard, L. F.; Lee, S.; Liu, J.; Li, H.; Wang, J.; Wang, J.; Oh, S. H.; Li, W. Surpassing the single-atom catalytic activity limit through paired Pt-O-Pt ensemble built from isolated Pt₁ atoms. *Nat. Commun.* **2019**, *10* (1), 3808.